Mitochondrial H$_2$S$_n$-Mediated Anti-Inflammatory Theranostics

Won Young Kim[1], Miae Won[1], Seyoung Koo[1], Xingcai Zhang[2,3], Jong Seung Kim[1] ✉

HIGHLIGHTS

- Theranostic agent **1** (**TA1**) was successfully developed to provide dual functions: anti-inflammatory therapy and precise diagnosis.

- **TA1** selectively reacts with H$_2$S$_n$ in the mitochondria in response to inflammatory reactions to simultaneously produce both indomethacin as a drug and ring-opened fluorescence-on Rhodol.

- Theranostic behavior of **TA1** was proven by in vitro and in vivo imaging.

- **TA1** reveals inflammatory site-selective drug release followed by significant therapeutic effects and is highly applicable in vivo model therapeutics for the inflammatory disease.

ABSTRACT The insistent demand for space-controllable delivery, which reduces the side effects of non-steroidal anti-inflammatory drugs (NSAIDs), has led to the development of a new theranostics-based approach for anti-inflammatory therapy. The current anti-inflammatory treatments can be improved by designing a drug delivery system responsive to the inflammatory site biomarker, hydrogen polysulfide (H$_2$S$_n$). Here, we report a novel
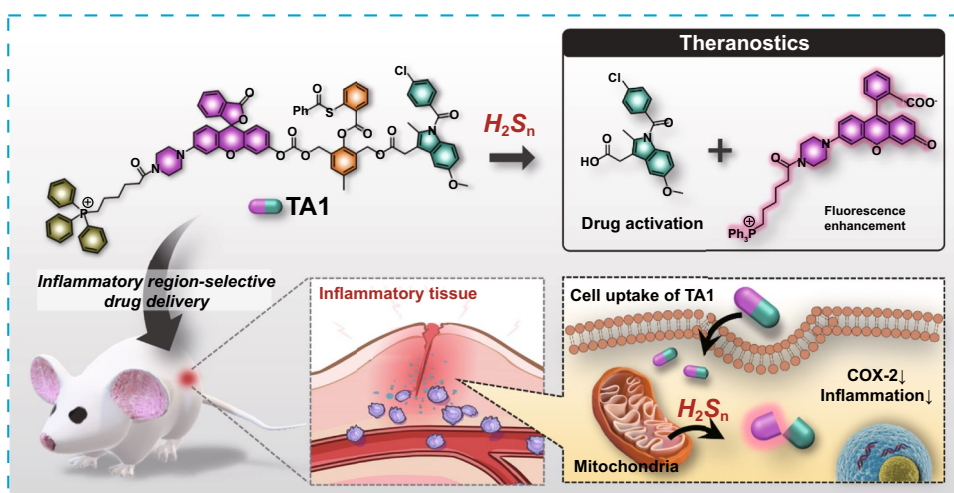
theranostic agent **1** (**TA1**), consisting of three parts: H$_2$S$_n$-mediated triggering part, a two-photon fluorophore bearing mitochondria targeting unit (Rhodol-TPP), and anti-inflammatory COX inhibitor (indomethacin). In vitro experiments showed that **TA1** selectively reacts with H$_2$S$_n$ to concomitantly release both Rhodol-TPP and indomethacin. Confocal-microscopy imaging of inflammation-induced

Won Young Kim, Miae Won, and Seyoung Koo contributed equally to this work.

✉ Jong Seung Kim, jongskim@korea.ac.kr

[1] Department of Chemistry, Korea University, Seoul 02841, Korea
[2] John A. Paulson School of Engineering and Applied Sciences, Harvard University, Cambridge, MA 02138, USA
[3] School of Engineering, Massachusetts Institute of Technology, Cambridge, MA 02139, USA

live cells suggested that **TA1** is localized in the mitochondria where the H_2S_n is overexpressed. The **TA1** reacted with H_2S_n in the endogenous and exogenous H_2S_n environments and in lipopolysaccharide treated inflammatory cells. Moreover, **TA1** suppressed COX-2 level in the inflammatory-induced cells and prostaglandin E_2 (PGE_2) level in blood serum from inflammation-induced mouse models. In vivo experiments with inflammation-induced mouse models suggested that **TA1** exhibits inflammation-site-elective drug release followed by significant therapeutic effects, showing its function as a theranostic agent, capable of both anti-inflammatory therapy and precise diagnosis. Theranostic behavior of **TA1** is highly applicable in vivo model therapeutics for the inflammatory disease.

1 Introduction

Inflammation is a biological response of body tissues to deleterious stimuli including injury, infection, damaged cells, pathogens, and irritants [1]. The immune system removes the injurious stimuli and initiates tissue repair through the inflammatory process [2]. Inflammation can be classified into two types: acute and chronic. Acute inflammation is an initial response to the harmful stimuli of the immune system, during which the movement of both plasma and white blood cells from the bloodstream to damaged tissues is increased, causing many biochemical events. This stage is accompanied by characteristic symptoms such as heat, pain, redness, swelling, and loss of tissue function in due course. Chronic inflammation, however, is long-term and leads to whole-body inflammation, producing steady and low-leveled inflammation throughout the body, which can develop from continuous acute inflammation [3]. This lasting chronic inflammation can eventually start markedly damaging tissues and organs, leading to the development of various chronic inflammatory diseases such as cardiovascular and bowel diseases, diabetes, arthritis, and cancer [4, 5]. Notably, it has been estimated that 15% of human cancers are associated with chronic inflammation [6].

Non-steroidal anti-inflammatory drugs (NSAIDs) exhibit excellent anti-inflammatory effects and are commonly prescribed medications to reduce pain, decrease fever, and prevent blood clots. NSAIDs reduce inflammation by inhibiting the activity of the cyclooxygenase enzymes (COX) involved in the synthesis of prostaglandins, which are key biological mediators in regulating inflammation [7]. Most NSAIDs are non-selective between COX-1 and COX-2. The NSAIDs inhibit COX-1 dependent generation of mucosal-protective gastric prostaglandins, thus considerably damaging the stomach and increasing the risk of gastrointestinal ulcers and bleeding, which are serious adverse effects of using NSAIDs. COX-2 selective inhibitors, on the other hand, exhibit lesser gastrointestinal side effects but cause thrombosis and substantially increase the risk of cardiovascular diseases [8]. These serious adverse effects are ascribed to the different roles and tissue localization of each COX isozyme. Due to these side effects of NSAIDs, there is an increasing demand for their selective delivery to specific inflammatory areas [9].

Hydrogen polysulfides (H_2S_n, $n > 1$) have drawn much attention because they are known as a fundamental regulator in biological redox-processes. Recent studies have suggested that the H_2S_n molecules engage in various physiological functions such as cellular signal transduction, redox biology, and cytoprotective processes [10–12]. Endogenous H_2S_n can be easily produced from the reaction of H_2S with reactive oxygen species (ROS) [13, 14]. In the body, the enzymes, cystathionine γ-lyase (CSE) and cystathionine-β-synthase (CBS), are able to produce H_2S, which can also generate persulfides that could, in turn, be converted into H_2S_n [15]. The H_2S_n thus generated is stored in mitochondria and can be released in response to physiological conditions such as oxidative stress and inflammation [16]. When inflammation occurs, the released H_2S_n plays a crucial role in cytoprotection by scavenging ROS and also promoting nuclear localization of Nrf2 (Nuclear factor erythroid 2-related factor 2), which is one of the regulators that enhance anti-oxidant genes [17, 18].

As H_2S_n is capable of triggering the selective delivery of anti-inflammatory drugs to inflammatory cells over normal cells, we for the first time designed H_2S_n-triggered anti-inflammatory theranostic agent **1** (**TA1**). "Theranostics" refers to the all-in-one system that integrates diagnostic and therapy, enabling precision and effective treatment. As seen in Scheme 1, the **TA1** consists of four crucial functional parts: aryl thioester as an exclusive H_2S_n reactive site over other biological species [19]; triphenylphosphonium (TPP) salt unit as a mitochondrion targeting part, considering that H_2S_n is mostly produced and stored in mitochondria;
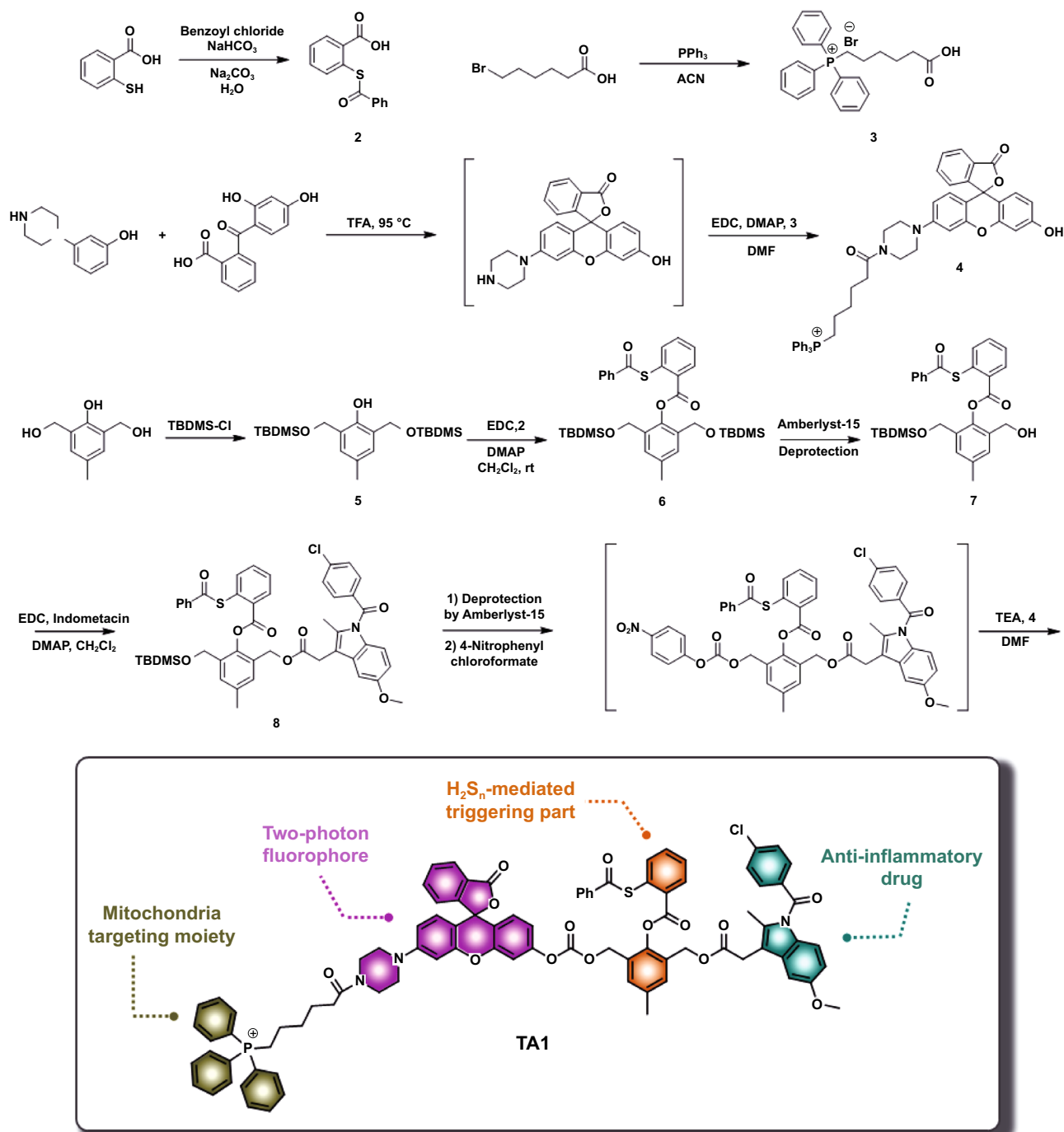
Scheme 1 Synthetic routes of **TA1** and schematic illustration of H_2S_n-mediated anti-inflammatory theranostics system

indomethacin as an anti-inflammatory drug able to inhibit COX enzyme that inhibits a synthesis of prostaglandins followed by reducing inflammation; and Rhodol dye as a fluorescent off–on reporter for the two-photon microscopy imaging. Such a theranostic system is a useful tool to visualize

the interaction of prodrug with certain biomarkers and provides useful information to assess the therapeutic efficacy, such as localization and release kinetics of the drug in situ. [20–27]. Two-photon dye utilizes a long-wavelength light as an excitation source to offer several advantages, such as

minimized tissue damage and deep tissue penetration, suitable for in vivo real-time bio-imaging [28–31].

Thus, in this system, the **TA1** can specifically localize in the inflammatory region, where the reaction of thioester moiety of the **TA1** with H_2S_n selectively takes place in mitochondria, which subsequently triggers the self-immolation reaction to concomitantly release both indomethacin and Rhodol-TPP. The self-immolation reaction can promote the ring-opening of the Rhodol compartment, which emits a strong fluorescence (off–on) in the inflammatory site. Simultaneously, the released indomethacin can lessen the corresponding inflammation without exhibiting adverse effects on normal cells. Therefore, it is notable that the novel H_2S_n-mediated **TA1** could provide a promising dual function of anti-inflammatory treatment and precise diagnosis, simultaneously, at the inflammation site.

2 Experimental

2.1 Materials

Unless otherwise noted, all the materials for the synthesis were purchased from commercial suppliers (Sigma-Aldrich, Alfa, Samchun) and were used without further purification. All the reactions were carried out under the nitrogen. All procedures for work-up and purification were carried out with reagent-grade solvents under ambient atmosphere. Column chromatography was performed with silica gel 60 (Merck, 0.063 ~ 0.2 mm) as a stationary phase. Analytical thin layer chromatography was performed using Merk 60 F254 silica gel (pre-coated sheets, 0.25 mm thick). ^1H and ^{13}C NMR spectra were collected in NMR solvent ($CDCl_3$) on a Bruker 500 MHz spectrometer. All chemical shifts are reported in ppm values using the peak of TMS as an internal reference. NMR data are reported as follows: chemical shifts, multiplicity (s: singlet, d: doublet, dd: doublet of doublets, t: triplet, q: quartet, m: multiplet, br: broad signal), and the coupling constant (Hz). The ESI-MS spectra were recorded using a Shimadzu LC/MS-2020 Series instrument and TSQ-LC-MS (Korea Basic Science Institute, Seoul).

2.2 Spectroscopic Measurements

UV/Vis spectra were recorded on a Scinco S-3100 spectrometer, and fluorescence spectra were obtained using a Shimadzu RF-5301PC instrument. Stock solutions of **TA1** were prepared in DMSO. All excitation and emission slit widths were set at 5 nm/3 nm. The concentration of each of the samples was fixed at 10 μM in a total volume of 3 mL.

2.3 HPLC Analysis

The aqueous solution of **TA1**, indomethacin, and Rhodol-TPP was prepared by mixing each compound (20 μM) in 10 mM PBS (pH 7.4). The reaction mixture of **TA1** with Na_2S_3 was prepared by mixing **TA1** (20 μM) and Na_2S_3 (200 μM) in 10 mM PBS (pH 7.4) containing cetrimonium bromide (200 μM; CTAB). Each sample was eluted at a flow rate of 1 mL/min using the mobile phase (Solvent A: deionized water containing 0.1% TFA, Solvent B: Methanol) with binary gradient (45–0% of Solvent A for 1 min, then 0% of Solvent A for 19 min, then 0–45% of Solvent A for 5 min). HPLC chromatogram was monitored using a 254 nm detector.

2.4 Cell Culture

Murine macrophage cell lines (RAW 264.7) were purchased from the Korean Cell Line Bank. Cells were cultured in DMEM containing high glucose (Hyclone) with 10% fetal bovine serum (GIBCO) and 1% antibiotics (penicillin–streptomycin) (GIBCO). Cells were maintained in a humidified atmosphere with 5% CO_2 at 37 °C.

2.5 Cell Viability Assay

RAW 264.7 cells (2×10^4 cells mL^{-1}) were seeded on a 96 well microplate (SPL Life Science) and cells to obtain approximately 80% confluence in 24 h. After incubation, the cells were treated with **TA1** and control containing 1% DMSO for 24 h. To investigate the cell viability of the RAW 264.7 cells treated with probes, we conducted a CytoTox96® Non-Radioactive Cytotoxicity Assay Kit (Promega) according to the protocol. The Absorbance was measured at 490 nm by a SPECTRA MAX microplate reader (Molecular Devices). Cell viability assays were performed 3 times in triplicate, and the cell viability (%) was calculated as a percentage of measured absorbance compared to the control cells with 1% DMSO.

2.6 One-photon Fluorescence Microscopy

RAW 264.7 Cells (5×10^5 cells) were seeded on confocal glass-bottom dishes (SPL Life Science) and cells to obtain approximately 80% confluence in 24 h. After stabilization, the cells were treated with **TA1** (10 μM with 1% DMSO) for 2 h at 37 °C. To monitor the effect of the exogenous increase of H_2S_n, cells were pre-incubated with 5 μM Na_2S_3 for 2 h before **TA1** treatment. To monitor the effect of the endogenous increase of H_2S_n, cells were pre-incubated with 10 μg/mL LPS (Escherichia coli 055:B5, 10 μg kg^{-1}, Sigma-Aldrich) for 16 h before **TA1** treatment. To monitor the effect of endogenous H_2S_n inhibition, cells were pre-incubated with 1.0 mM PAG (DL-propargyl-glycine, Sigma-Aldrich, P7888) for 8 h before **TA1** treatment. After cells were washed with PBS, mitochondria was stained using a MitoTracker Red^{FM} (Invitrogen, USA) for 30 min. After incubation, cells were washed with PBS 3 times. One-photon fluorescence images were obtained by the probes with a confocal laser scanning microscope (Carl-Zeiss LSM 700). The fluorescence channel of **TA1** was excited at 488 nm, and the emission was collected by 500–600 nm.

2.7 Two-photon Fluorescence Microscopy

RAW 264.7 Cells (5×10^5 cells) were seeded on confocal glass-bottom dishes (SPL Life Science) and cells to obtain approximately 80% confluence in 24 h. After stabilization, the cells were treated with **TA1** (10 μM with 1% DMSO) for 2 h at 37 °C. The two-photon fluorescence microscopy images were obtained by exciting the probes with a spectral confocal microscope (Leica TCS SP2) with a mode-locked titanium-sapphire laser source (Coherent Chameleon) set at wavelength 800 nm in the focal plane in $\times 100$ oil (NA $= 1.30$) objective lens. To obtain images at 500–600 nm range, internal PMTs were used to obtain the signals in an 8 bit unsigned 512×512 pixels at 400 Hz scan speed.

2.8 Fluorescence Imaging of Acute Liver Injury in Mice Models

C57Bl/6 male mice (8 weeks old) were obtained from Orientbio (Seoul, Korea) and were established for the acute liver injury model using LPS. Animal care and experiments were conducted following guidelines by Korea University Institutional Animal Care Use Committee (KUIACUC No. 201900090). Mice were *i.v.* injected with a freshly prepared **TA1** solution (10 mg kg^{-1}, in 5% DMSO) for 30 min. Then, 5% DMSO or LPS was intraperitoneally injected. At indicated time point, fluorescence images were collected at the indicated time point in vivo imaging machine (Maestro, CRi Inc., Woburn, MA, USA) with an emission filter from 550 to 750 nm (orange channel).

2.9 ELISA Assay

Blood plasma was collected at the indicated time point, to conduct plasma enzymes and cytokines analysis in mice. Plasma activity of alanine aminotransferase (ALT) and aspartate aminotransferase (AST), as markers of hepatic damage; TNF-α and IL-1β, as markers of pro-inflammatory factors; PGE_2, as a marker of COX-2 product at inflammatory sites were analyzed by an Enzyme-Linked Immunosorbent Assay Kit (Invitrogen.). Each enzyme activity signal was measured using a Multi-Detection Microplate Reader system (HIDEX), following the manufacturer's procedure.

2.9.1 Statistical Analysis

The data of statistical significance represent the mean $\pm$ S.E. The data were analyzed by SAS 9.4 ver. Statistical significance was determined by a two-way ANOVA test with a Bonferroni test and Student's t-test. Different letters statistically distinct signify data sets. ($p < 0.05$).

3 Results and Discussion

3.1 Synthesis of TA1

As shown in Scheme 1, the structure of target molecule **TA1** comprises three parts: 1) H_2S_n-reactive triggering part, 2) Rhodol-based two-photon fluorophore bearing mitochondria targeting TPP, and 3) anti-inflammatory drug, indomethacin. The **TA1** was synthesized by the following procedure. First, H_2S_n-reactive site **2** was prepared by s-acetylation of thiosalicylic acid using benzoyl chloride. The triggering unit, **6**, was synthesized via *tert*-butyldimethyl silyl (TBDMS) protection at both sides of aliphatic hydroxyl group of 2,6-bis(hydroxymethyl)-*p*-cresol, followed by 1-ethyl-3-(3-dimethylaminopropyl)carbodiimide (EDC)
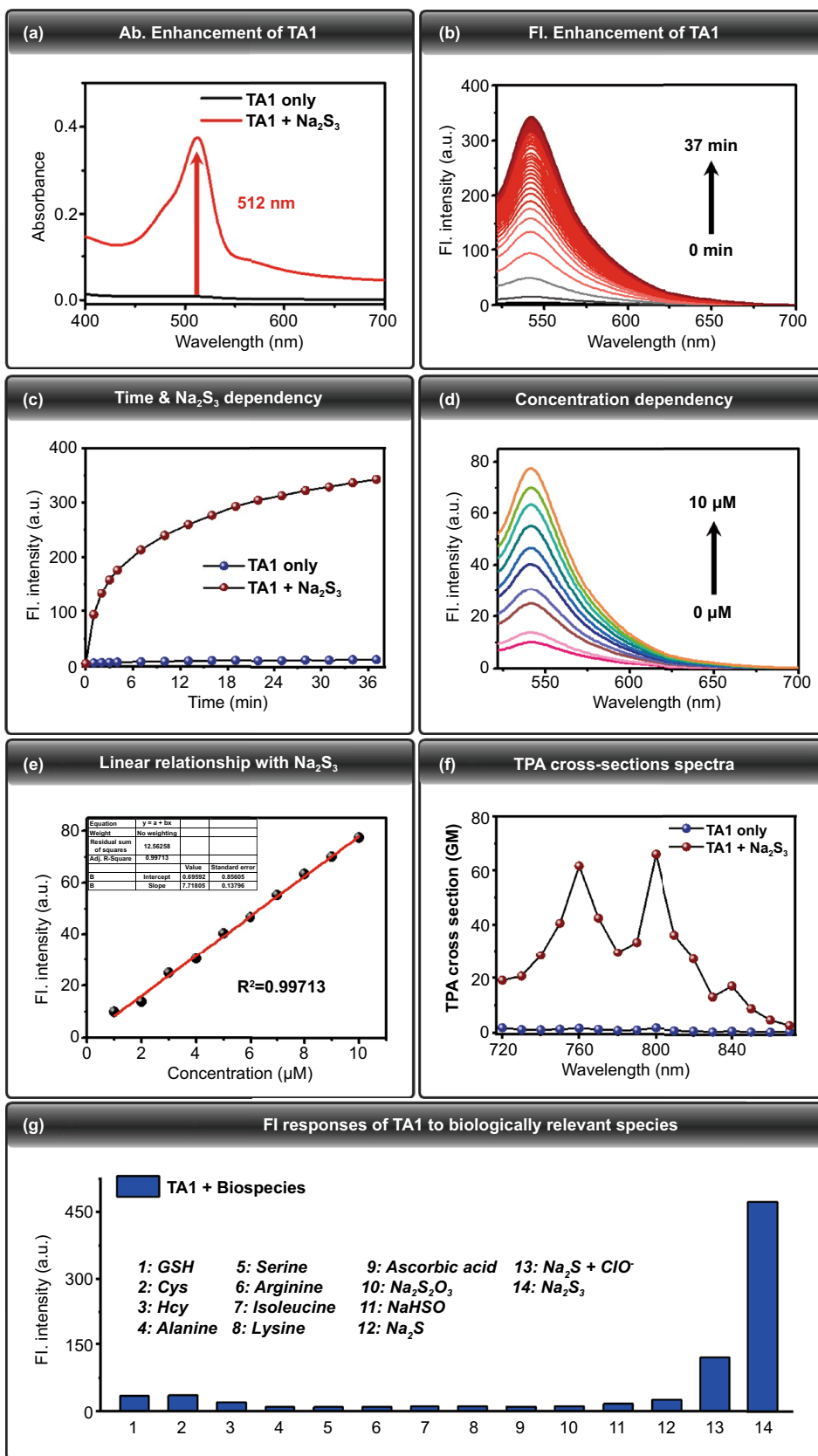
◄**Fig. 1 a** Absorbance spectra of **TA1** (10 μM) in the absence of Na$_2$S$_3$ (black line), upon addition of Na$_2$S$_3$ (red line) (100 μM, 10 mM PBS buffer, 0.2% DMSO, 100 μM CTAB). **b** Time-dependent fluorescence spectral changes of **TA1** (10 μM) $\lambda_{ex} = 512$ nm, $\lambda_{em} = 542$ nm, upon addition of Na$_2$S$_3$ (100 μM, 10 mM PBS buffer, 0.2% DMSO, 100 μM CTAB). **c** Fluorescence intensity changes of **TA1** (10 μM) in the absence of Na$_2$S$_3$ (blue sphere), upon addition of Na$_2$S$_3$ (red sphere). **d** Fluorescence responses of **TA1** (10 μM) toward addition of a range of concentrations of Na$_2$S$_3$ (0 to 10 μM). **e** Linear relationship between the fluorescence intensity and Na$_2$S$_3$ concentrations. Data were acquired in 10 mM PBS buffer (0.2% DMSO, 100 μM CTAB) after incubation with Na$_2$S$_3$ for 2 min at 37 °C. $\lambda_{ex} = 512$ nm, $\lambda_{em} = 542$ nm. **f** Two-photon absorption (TPA) cross-sections spectra of **TA1** (10 μM) upon addition of Na$_2$S$_3$ (100 μM, 10 mM PBS buffer, 0.5% DMSO, 100 μM CTAB). **g** Fluorescence responses of **TA1** (10 μM) to biologically relevant species. Each bar represents fluorescence increases of **TA1** at 542 nm to 100 μM Na$_2$S$_3$ or other species. 1) 1 mM GSH; 2) 500 μM Cys; 3) 500 μM Hcy; 4) 100 μM Alanine; 5) 100 μM Serine; 6) 100 μM Arginine; 7) 100 μM Isoleucine; 8) 100 μM Lysine; 9) 100 μM Ascorbic acid; 10) 100 μM Na$_2$S$_2$O$_3$; 11) 100 μM NaHSO$_3$; 12) 100 μM Na$_2$S; 13) 100 μM Na$_2$S + 50 μM ClO$^-$; 14) 100 μM Na$_2$S$_3$. The data were acquired in 10 mM PBS buffer (0.2% DMSO, 100 μM CTAB) after incubation for 30 min. $\lambda_{ex} = 512$ nm. (Color figure online)

coupling reaction with **2**. Then, the mono-deprotection of the TBDMS group in **6** was conducted in the presence of amberlyst-15 to yield **7**. Compound **7** was then conjugated with indomethacin through EDC coupling to produce **8**. Finally, the other TBDMS group of **8** was further deprotected using amberlyst-15 and subsequently reacted with 4-nitrophenyl chloroformate for activation. The resulting intermediate was reacted with TPP-conjugated two-photon Rhodol fluorophore **4** (Rhodol-TPP) which was synthesized by EDC coupling of Rhodol and **3**, successfully yielding the desired product, **TA1** (Scheme 1). The detailed procedures of the synthesis and structurally characterized evidence for the compounds are provided in supporting information.

3.2　Characterization of TA1

To determine whether **TA1** could react with H$_2$S$_n$ to give an off–on fluorescence change, the photophysical change of **TA1** (10 μM) was investigated using UV–Vis absorption and fluorescence spectroscopy under simulated physiological conditions (10 mM PBS buffer, pH 7.4), in the presence and absence of Na$_2$S$_3$ (100 μM), H$_2$S$_n$ donor. UV–Vis absorption intensity of **TA1** (10 μM) markedly enhanced at 512 nm upon addition of Na$_2$S$_3$ (100 μM, 10 mM PBS buffer, 0.2% DMSO, 100 μM CTAB) (Fig. 1a). Time-dependent fluorescence intensity changes of **TA1** (10 μM) were observed, and

they indicated a marginal fast (30 min) and gradual increase of its fluorescence intensity at 542 nm, upon treatment with Na$_2$S$_3$ (Fig. 1b, c). These results confirm that the **TA1** reacts with H$_2$S$_n$ and induces cleavage of H$_2$S$_n$-reactive triggering part to release the corresponding fluorophore, where the fluorescence off–on change is attributed to the ring-opening of Rhodol fluorophore upon self-immolation reaction (Fig. 2a). The fluorescence responses of **TA1** (10 μM) to H$_2$S$_n$ were also evaluated to investigate the sensitivity to different concentrations of Na$_2$S$_3$ (0 to 10 μM). As a function of Na$_2$S$_3$ concentration, gradually increasing fluorescence intensity of **TA1** ($\lambda_{ex} = 512$ nm) was observed, with a center at 542 nm (Fig. 1d). A linear correlation of various concentrations of Na$_2$S$_3$ with fluorescence intensities at 542 nm was also observed (Fig. 1e). Taken together, we conclude that **TA1** can effectively respond to H$_2$S$_n$ with reliable sensitivity under physiological conditions.

For two-photon confocal-microscopic imaging of the probe, TPA cross sections of **TA1** and **TA1** + H$_2$S$_n$ were initially investigated with rhodamine 6G as the reference molecule. Upon addition of Na$_2$S$_3$ (100 μM), **TA1** exhibited 66 GM with maximum TPA cross-section value at 800 nm under physiological conditions (PBS buffer, 0.5% DMSO, 100 μM CTAB), which validates that **TA1** can be sufficiently sensitized by two-photon absorption (Fig. 1f).

To determine the selectivity of **TA1** toward H$_2$S$_n$ over other biological species, fluorescence experiments with a series of other biologically relevant species were also performed. The **TA1** showed a high selectivity for Na$_2$S$_3$ over amino acids and other nucleophilic sulfur species such as glutathione (GSH), cysteine (Cys), homocysteine (Hcy), S$_2$O$_3$$^{2-}$, HSO$_3$$^-$, and Na$_2$S (Fig. 1g). Moreover, **TA1** was also found to be inert to other reductive species such as ascorbic acid. Upon treatment of a mixed solution of Na$_2$S (200 μM) and ClO$^-$ (50 μM) to generate H$_2$S$_n$ in situ, **TA1** showed a strongly enhanced fluorescence at 542 nm as well. These results conclude that **TA1** can selectively respond to H$_2$S$_n$ in the biological media containing various potential interferences.

3.3　Proposed Mechanism of H$_2$S$_n$-responsive Activation of TA1

To verify that the proposed self-immolation cleavage mechanism of the theranostics system shown in Fig. 2a is
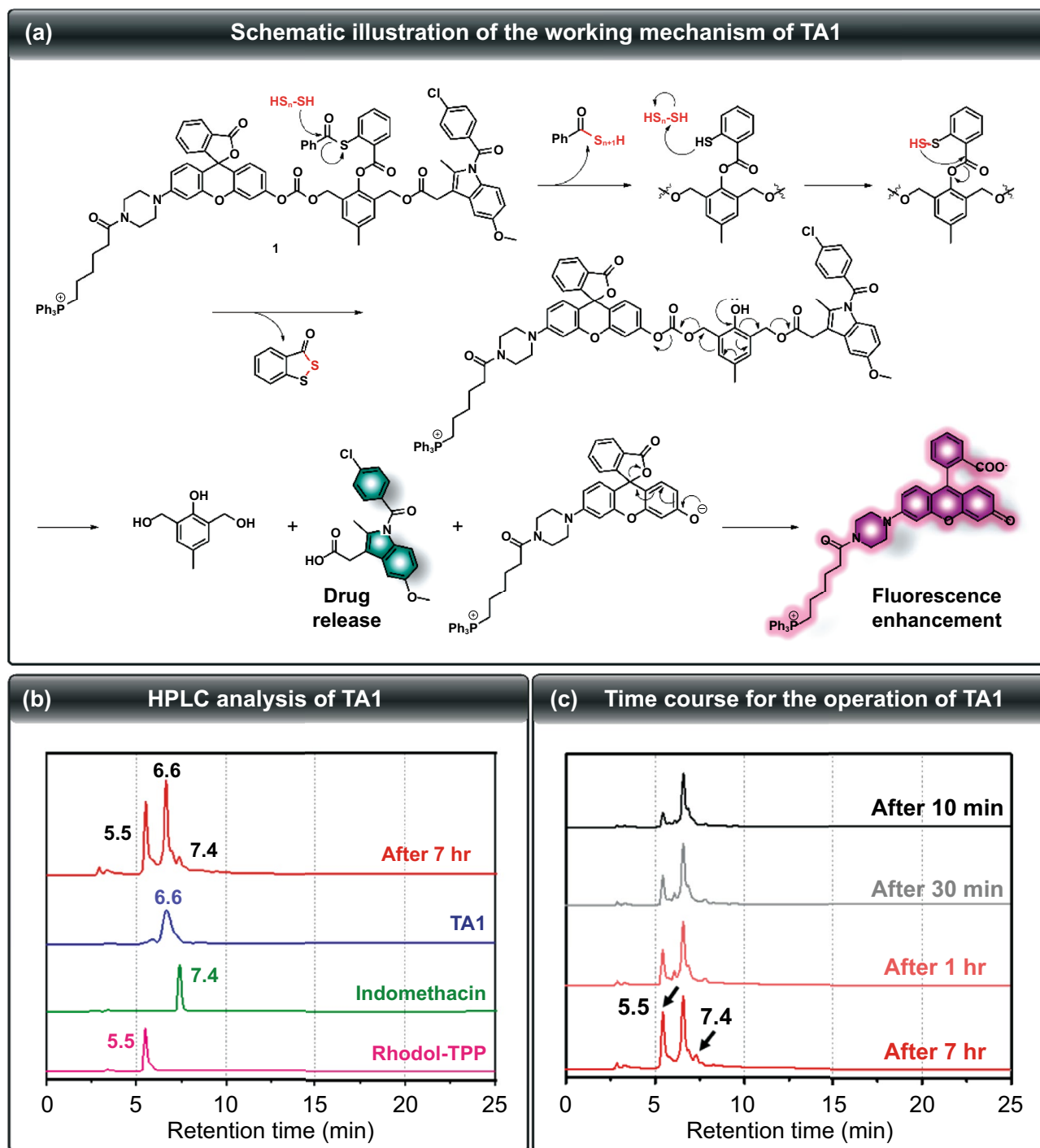
Fig. 2 **a** Schematic illustration of the working mechanism of **TA1**. **b** HPLC chromatogram of **TA1** (blue line), indomethacin (green line), Rhodol-TPP (pink line), and the reaction mixture of **TA1** with Na_2S_3 (red line). **c** Time-dependent change of HPLC chromatogram of the reaction mixture of **TA1** with Na_2S_3. (COlor figure online)

reasonably operated, HPLC analysis of **TA1** in the presence of Na_2S_3 was undertaken. As shown in Fig. 2b, the retention time for **TA1**, Rhodol-TPP, and indomethacin was

6.6, 5.5, and 7.4 min, respectively. Time-course experiment upon reaction with H_2S_n gave a Rhodol-TPP peak, cleaved from **TA1**, which gradually increased. Indomethacin release

began after 1 h, indicating that **TA1** can release both Rhodol-TPP and indomethacin, simultaneously, upon reaction with H_2S_n (Fig. 2c). Moreover, the ESI–MS spectrum of **TA1** in the presence of Na_2S_3 showed two peaks of m/z 380.12 and 759.30, corresponding to indomethacin and Rhodol-TPP, respectively (Fig. S13). This result supports the mode of action that **TA1** simultaneously releases both indomethacin and Rhodol-TPP in the presence of H_2S_n.

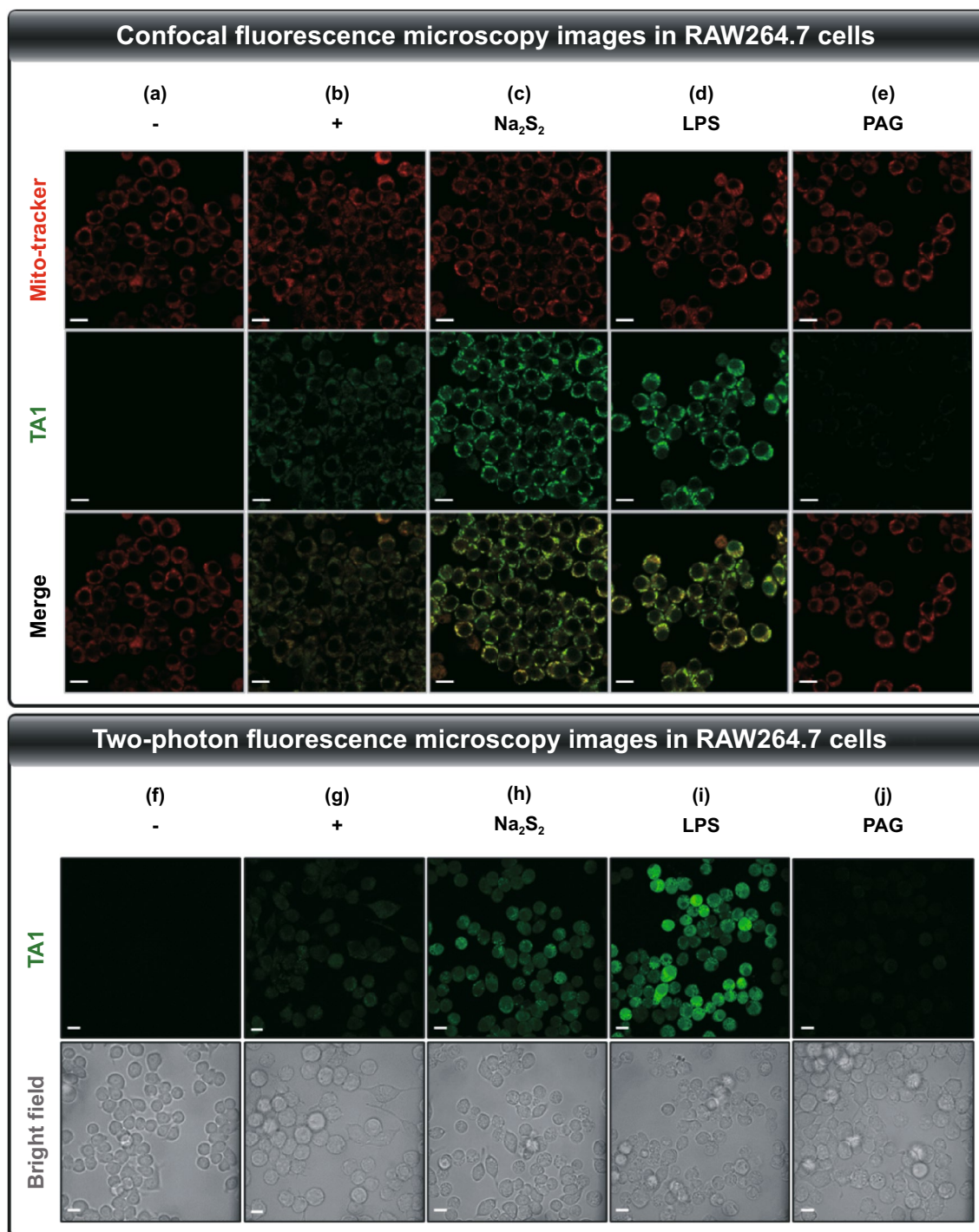## 3.4 Selective Activation of TA1 in vitro

The abovementioned results suggest that **TA1** selectively reacts with H_2S_n and could be suitable for precise drug delivery as a potential theranostic agent. The **TA1** was then applied to mouse macrophage cell line, RAW264.7, as a bioassay model. First, from the LDH cytotoxicity assay, we found the low cytotoxicity of **TA1** in RAW264.7 cells, at various concentrations after 24 h-incubation (Fig. S14), thus suggesting that it could be further applied to an anti-inflammatory therapeutic system. Subsequently, confocal-microscopy images of the live RAW264.7 cells having endogenous H_2S_n were obtained in the presence of **TA1** (10 µM) at 37 °C. The group treated with **TA1** exhibited brighter fluorescence as it responded to H_2S_n compared to that exhibited by the control group (Fig. 3a, b and S15). The group further treated with exogenous Na_2S_2 (5 µM) displayed stronger fluorescence (Fig. 3c and S15). To further examine the responsiveness to endogenously produced H_2S_n by perturbing the pool, RAW264.7 cells were pre-incubated with LPS (1 µg mL^{-1}, 16 h), which can induce an inflammatory environment to trigger the overexpression of CSE mRNA, and thus promote the production of endogenous H_2S_n. Upon subsequent treatment of **TA1** (10 µM, 2 h), the cells displayed a remarkable increase in fluorescence intensity (Fig. 3d and S15).

On the contrary, the pretreatment of DL-propargylglycine (PAG, 1 mM; CSE inhibitor) significantly attenuated the fluorescence intensity of **TA1**, thus confirming that CSE contributed to the endogenous generation of H_2S_n (Fig. 3e and S15). Moreover, mitochondrial localization of **TA1** was demonstrated via co-localization assays with Mito-tracker Red (Fig. 3b-e and S16), thereby proving the accessibility of **TA1** to mitochondrial H_2S_n. In addition, two-photon fluorescence microscopy images were collected from RAW264.7 cells for investigating the responsiveness of **TA1** toward

H_2S_n upon excitation at 800 nm (Fig. 3f-j and S15). These results are consistent with those from the one-photon fluorescence microscopy experiment. Collectively, the results thus indicate that **TA1** can react with endogenous cellular H_2S_n in living cells, which can be directly visualized by fluorescence off–on changes with both one-photon and two-photon fluorescence microscopy.

3.5 Anti-inhibitory Effects of TA1 in vivo

Following the results that **TA1** selectively responds to endogenous and exogenous H_2S_n in living cells and shows diagnostic abilities, the therapeutic effect of **TA1** against inflammation was subsequently investigated by various biological tests. First, the western blot analysis of inflammation-induced RAW264.7 cells treated by LPS was implemented to explore COX-2 levels. The group treated with LPS exhibited high expression of COX-2 levels and another group treated with *N*-Acetyl cysteine (NAC, 1 mM for 12 h), a quencher of LPS-mediated inflammation, displayed decreased COX-2 levels (Fig. 4a). However, cells incubated with further treatment of **TA1** exhibited a significant reduction of COX-2 expression compared to that in the control group. This result signifies that **TA1** selectively releases indomethacin (IMC) upon reaction with H_2S_n, existing in the inflammatory environment, to reduce COX-2 levels. We also observed that PGE_2 production increased in LPS-induced inflammatory response, whereas the levels were markedly reduced in **TA1** treated RAW264.7 cells (Fig. 4b). Moreover, an inflammation-induced mouse model was established to confirm the in vivo theranostic potential of **TA1**. Ahead of investigation, LPS was intraperitoneally injected in mice to cause hepatotoxicity and inflammation. Upon the injection of **TA1** into the LPS-induced acute liver injury (ALI) mouse model, the fluorescence expressions were observed to verify whether **TA1** is triggered at the inflammatory site. As seen in Fig. 4c and S17, the marked fluorescence enhancement of in vivo and ex vivo imaging was observed in the liver because **TA1** released both Rhodol-TPP and IMC upon reaction with H_2S_n at the inflammatory site. Besides, the blood serum of the ALI mouse model was isolated to examine PGE_2 level, which is representative of the level of inflammation. As shown in Fig. 4d, the PGE_2 level in the ALI mouse model was significantly high, whereas it was reduced in the serum of the mice treated with either **TA1** or IMC. To investigate

Confocal fluorescence microscopy images in RAW264.7 cells

Two-photon fluorescence microscopy images in RAW264.7 cells

Fig. 3 Confocal fluorescence microscopy images in RAW264.7 cells incubated with **TA1** (10 μM) for 2 h. The cells in each group were subjected to different treatments. **a** Control (1% DMSO), **b** TA1, **c** TA1+Na$_2$S$_2$ (5 μM), **d** TA1+LPS (1 μg mL^{-1}), **e** TA1+PAG (1 mM). Fluorescence images of cells were collected at $\lambda_{ex}=488$ nm, $\lambda_{em}=500$–560 nm of **TA1** and at $\lambda_{ex}=579$ nm, $\lambda_{em}=580$–620 nm of Mito-tracker. Two-photon fluorescence microscopy images in RAW264.7 cells incubated with **TA1** (10 μM) for 2 h. The cells in each group were subjected to different treatments. **f** Control (1% DMSO), **g** TA1, **h** TA1+Na$_2$S$_2$ (5 μM), **i** TA1+LPS (1 μg mL^{-1}), **j** TA1+PAG (1 mM). Fluorescence images of cells were collected at $\lambda_{ex}=800$ nm, $\lambda_{em}=500$–600 nm. Scale bar = 100 μm
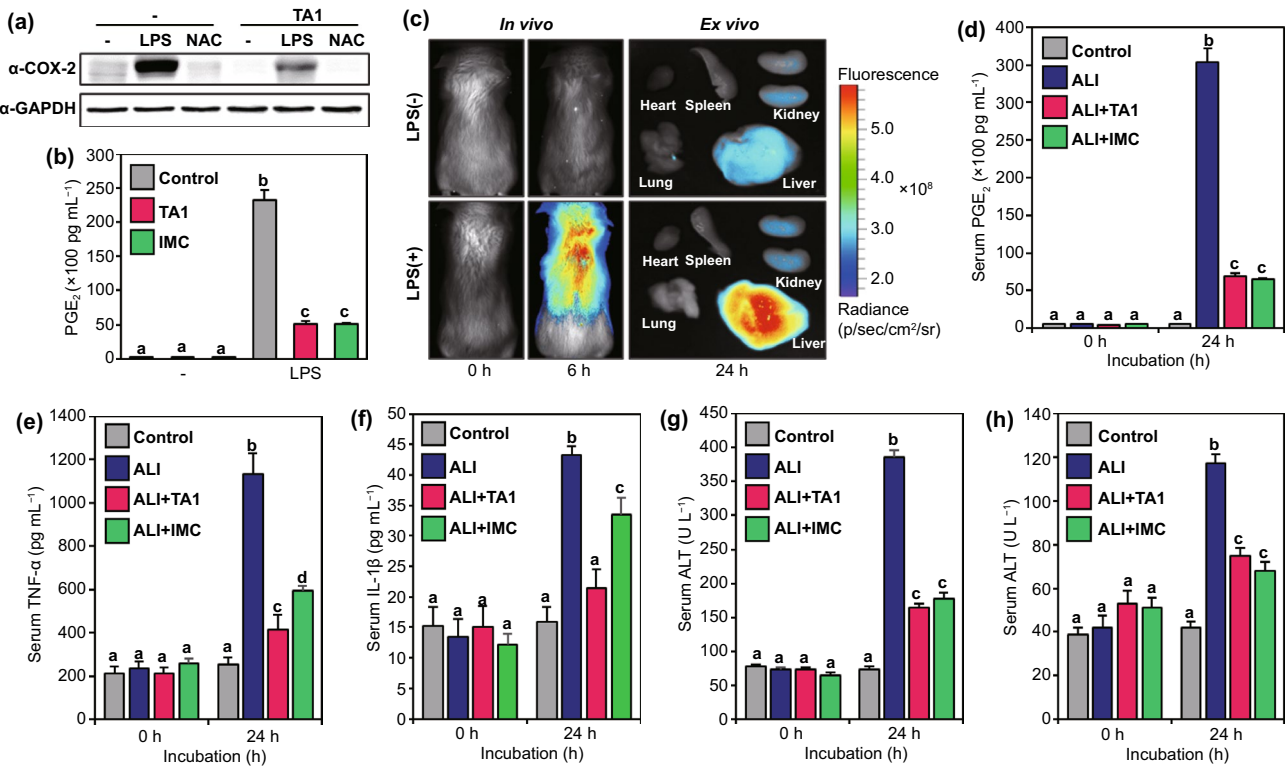
Fig. 4 Anti-inflammatory effects of **TA1**. **a** Western blotting analysis of COX-2 protein in RAW264.7 cells. Cells were pre-incubated with LPS or NAC for 16 h before **TA1** treatment. **b** PGE_2 levels of inflammation-induced RAW264.7 cells by LPS. **c** In vivo and ex vivo imaging of ALI mouse model. Mice were *i.v.* injected with **TA1** for 30 min and then treated with either 5% DMSO or LPS (10 µg kg^{-1}). **d** Serum PGE_2 levels of ALI mouse model. Levels of pro-inflammatory cytokines **e** TNF-α and **f** IL-1β on blood collected at indicated time points (0 and 24 h) after LPS (*i.p.*) administration. Levels of hepatic toxicity markers **g** AST and **h** ALT on blood collected at indicated time points (0 and 24 h) after LPS (*i.p.*) administration. Control (5% DMSO), ALI (LPS 10 µg kg^{-1}), ALI + **TA1** (10 µg kg^{-1} LPS, 10 mg kg^{-1} **TA1**) and ALI + IMC (10 µg kg^{-1} LPS, 10 mg kg^{-1} IMC). Statistical significance was determined by a two-way ANOVA test with a post-hoc Bonferroni test. Different letters (*e.g.,* **a–d**) signify data sets that are statistically distinct ($p < 0.05$). ALI: LPS-induced acute liver injury, IMC: indomethacin, AST: aspartate transaminase, ALT: alanine aminotransferase

anti-inflammatory effects in the ALI mouse model, we further analyzed the production of pro-inflammatory cytokines, such as TNF-α and IL-1β in serum. The levels of TNF- α and IL-1β increased for 24 h in the ALI mouse model; however, the levels were significantly decreased in the group treated with **TA1** or IMC (Fig. 4e, f and S18). We also confirmed that **TA1** overcomes inflammatory responses, suppressing plasma levels of alanine aminotransferase (ALT) and aspartate aminotransferase (AST) in ALI mouse models (Fig. 4g, h). These results strongly suggest that the theranostic agent **TA1**, developed for the first time in this study, can selectively treat inflammation-related diseases by releasing the corresponding drug to the inflammatory site exclusively upon reaction with H_2S_n and, simultaneously, aid in the diagnosis of the inflammation by fluorescence imaging in vivo.

4 Conclusions

In summary, a novel H_2S_n mediated anti-inflammatory theranostic agent, **TA1**, was developed to selectively deliver the NSAID, indomethacin, to the inflammatory region and to visualize the inflammation site using fluorescence off–on imaging of Rhodol-TPP by triggering H_2S_n. In this study, we found that **TA1** exerts a selectivity to H_2S_n over other biological species such as amino acids and other reactive oxygen species, and the fluorescence signal of **TA1** is markedly enhanced not only in the endogenous and exogenous H_2S_n environments but also in the inflammation-induced RAW264.7 cells by LPS. In addition, **TA1** exhibited the ability of two-photon excited fluorescence imaging, which is highly applicable to in vitro and in vivo biological

experiments. Furthermore, we found that **TA1** could suppress both COX-2 level in the live cells and PGE$_2$ level in blood serum, which are factors associated with inflammation-induced mouse models where H$_2$S$_n$ is overexpressed. Therefore, these results strongly suggest that **TA1,** we have first discovered has potential as a new theranostic agent as it is highly applicable to in vivo model therapeutics for inflammatory diseases.

Supplementary Information The online version contains supplementary material available at https://doi.org/10.1007/s40820-021-00689-1.

References

1. R. Medzhitov, Inflammation 2010: New adventures of an old flame. Cell **140**, 771–776 (2010). https://doi.org/10.1016/j.cell.2010.03.006
2. Y. Wang, D. Gao, Y. Liu, X. Guo, S. Chen et al., Immunogenic-cell-killing and immunosuppression-inhibiting nanomedicine. Bioact. Mater. **6**, 1513–1527 (2021). https://doi.org/10.1016/j.bioactmat.2020.11.016
3. O. Takeuchi, S. Akira, Pattern recognition receptors and inflammation. Cell **140**, 805–820 (2010). https://doi.org/10.1016/j.cell.2010.01.022
4. J. Ouyang, X. Ji, X. Zhang, C. Feng, Z. Tang et al., In situ sprayed NIR-responsive, analgesic black phosphorus-based gel for diabetic ulcer treatment. Proc. Natl. Acad. Sci. USA **117**, 28667–28677 (2020). https://doi.org/10.1073/pnas.2016268117
5. M.A. Sugimoto, L.P. Sousa, V. Pinho, M. Perretti, M.M. Teixeira, Resolution of inflammation: What controls its onset?
6. G. He, M. Karin, Nf-kappab and stat3 - key players in liver inflammation and cancer. Cell Res. **21**, 159–168 (2011). https://doi.org/10.1038/cr.2010.183
7. S. Crittenden, M. Goepp, J. Pollock, C.T. Robb, D.J. Smyth et al., Prostaglandin E2 promotes intestinal inflammation via inhibiting microbiota-dependent regulatory T cells. Sci. Adv. **7**, 7954 (2021). https://doi.org/10.1126/sciadv.abd7954
8. A.M. Schjerning, P. McGettigan, G. Gislason, Cardiovascular effects and safety of (non-aspirin) NSAIDs. Nat. Rev. Cardiol. **17**, 574–584 (2020). https://doi.org/10.1038/s41569-020-0366-z
9. J. Tan, Z. Deng, G. Liu, J. Hu, S. Liu, Anti-inflammatory polymersomes of redox-responsive polyprodrug amphiphiles with inflammation-triggered indomethacin release characteristics. Biomaterials **178**, 608–619 (2018). https://doi.org/10.1016/j.biomaterials.2018.03.035
10. M. Peleli, S.I. Bibli, Z. Li, A. Chatzianastasiou, A. Varela et al., Cardiovascular phenotype of mice lacking 3-mercaptopyruvate sulfurtransferase. Biochem. Pharmacol. **176**, 113833 (2020). https://doi.org/10.1016/j.bcp.2020.113833
11. H. Kimura, Signaling molecules: Hydrogen sulfide and polysulfide. Antioxid. Redox Signal. **22**, 362–376 (2015). https://doi.org/10.1089/ars.2014.5869
12. E.C. Estevam, L. Faulstich, S. Griffin, T. Burkholz, C. Jacob, Polysulfides in biology: From intricate chemistry to an astonishing yet hidden biological activity. Curr. Org. Chem. **20**, 211–217 (2016). https://doi.org/10.2174/1385272819666150724233028
13. H. Dong, Q. Zhou, L. Zhang, Y. Tian, Rational design of specific recognition molecules for simultaneously monitoring of endogenous polysulfide and hydrogen sulfide in the mouse brain. Angew. Chem. Int. Ed. **58**, 13948–13953 (2019). https://doi.org/10.1002/anie.201907210
14. P. Nagy, Z. Palinkas, A. Nagy, B. Budai, I. Toth et al., Chemical aspects of hydrogen sulfide measurements in physiological samples. Biochim. Biophys. Acta **1840**, 876–891 (2014). https://doi.org/10.1016/j.bbagen.2013.05.037
15. P.K. Yadav, M. Martinov, V. Vitvitsky, J. Seravalli, R. Wedmann et al., Biosynthesis and reactivity of cysteine persulfides in signaling. J. Am. Chem. Soc. **138**, 289–299 (2016). https://doi.org/10.1021/jacs.5b10494
16. M.R. Jackson, S.L. Melideo, M.S. Jorns, Human sulfide: Quinone oxidoreductase catalyzes the first step in hydrogen sulfide metabolism and produces a sulfane sulfur metabolite. Biochemistry **51**, 6804–6815 (2012). https://doi.org/10.1021/bi300778t
17. V.S. Lin, A.R. Lippert, C.J. Chang, Cell-trappable fluorescent probes for endogenous hydrogen sulfide signaling and imaging H$_2$O$_2$-dependent H$_2$S production. Proc. Natl. Acad. Sci. USA **110**, 7131–7135 (2013). https://doi.org/10.1073/pnas.1302193110
18. N. Gupta, S.I. Reja, V. Bhalla, M. Kumar, Fluorescent probes for hydrogen polysulfides (H$_2$S$_n$, n > 1): From design rationale

Front. Immunol. **7**, 160 (2016). https://doi.org/10.3389/fimmu.2016.00160

to applications. Org. Biomol. Chem. **15**, 6692–6701 (2017). https://doi.org/10.1039/c7ob01615h

19. W. Chen, E.W. Rosser, T. Matsunaga, A. Pacheco, T. Akaike et al., The development of fluorescent probes for visualizing intracellular hydrogen polysulfides. Angew. Chem. Int. Ed. **54**, 13961–13965 (2015). https://doi.org/10.1002/anie.201506887

20. W. Chen, C.R. Liu, B. Peng, Y. Zhao, A. Pacheco et al., New fluorescent probes for sulfane sulfurs and the application in bioimaging. Chem. Sci. **4**, 2892–2896 (2013). https://doi.org/10.1039/c3sc50754h

21. S. Park, E. Kim, W.Y. Kim, C. Kang, J.S. Kim, Biotin-guided anticancer drug delivery with acidity-triggered drug release. Chem. Commun. **51**, 9343–9345 (2015). https://doi.org/10.1039/c5cc03003j

22. W.Y. Kim, H. Shi, H.S. Jung, D. Cho, P. Verwilst et al., Coumarin-decorated schiff base hydrolysis as an efficient driving force for the fluorescence detection of water in organic solvents. Chem. Commun. **52**, 8675–8678 (2016). https://doi.org/10.1039/c6cc04285f

23. H.S. Jung, J. Han, H. Shi, S. Koo, H. Singh et al., Overcoming the limits of hypoxia in photodynamic therapy: A carbonic anhydrase ix-targeted approach. J. Am. Chem. Soc. **139**, 7595–7602 (2017). https://doi.org/10.1021/jacs.7b02396

24. N.K. Hien, D.T. Nhan, W.Y. Kim, M. Van Bay, P.C. Nam et al., Exceptional case of kasha's rule: Emission from higher-lying singlet electron excited states into ground states in coumarin-based biothiol sensing. Dyes. Pigm. **152**, 118–126 (2018). https://doi.org/10.1016/j.dyepig.2018.01.046

25. M.S. Chowdhury, W. Zheng, S. Kumari, J. Heyman, X. Zhang et al., Dendronized fluorosurfactant for highly stable water-in-fluorinated oil emulsions with minimal inter-droplet transfer of small molecules. Nat. Commun. **10**, 4546 (2019). https://doi.org/10.1038/s41467-019-12462-5

26. T. He, X. Qin, C. Jiang, D. Jiang, S. Lei et al., Tumor pH-responsive metastable-phase manganese sulfide nanotheranostics for traceable hydrogen sulfide gas therapy primed chemodynamic therapy. Theranostics **10**, 2453–2462 (2020). https://doi.org/10.7150/thno.42981

27. Z. Li, Y. Hu, Z. Miao, H. Xu, C. Li et al., Dual-stimuli responsive bismuth nanoraspberries for multimodal imaging and combined cancer therapy. Nano Lett. **18**, 6778–6788 (2018). https://doi.org/10.1021/acs.nanolett.8b02639

28. K.N. Bobba, M. Won, I. Shim, N. Velusamy, Z.G. Yang et al., A bodipy-based two-photon fluorescent probe validates tyrosinase activity in live cells. Chem. Commun. **53**, 11213–11216 (2017). https://doi.org/10.1039/c7cc05043g

29. A. Podder, M. Won, S. Kim, P. Verwilst, M. Maiti et al., A two-photon fluorescent probe records the intracellular ph through "or" logic operation via internal calibration. Sens. Actuat. B **268**, 195–204 (2018). https://doi.org/10.1016/j.snb.2018.04.092

30. N.Y. Lim, J. Ahn, M. Won, W. Choi, J.S. Kim et al., Novel cyanostilbene-based fluorescent chemoprobe for hydroxyl radicals and its two-photon bioimaging in living cells. ACS Appl. Bio Mater. **2**, 936–942 (2019). https://doi.org/10.1021/acsabm.8b00796

31. H.M. Kim, B.R. Cho, Small-molecule two-photon probes for bioimaging applications. Chem. Rev. **115**, 5014–5055 (2015). https://doi.org/10.1021/cr5004425